CHEMISTRY OF MATERIALS

ARTICLE

pubs.acs.org/cm

Influence of the Alkyl Mantle on the Self-Assembly of Phenylene−Thienylene-Based Oligomers

Alexey Mavrinskiy,[†] Christian B. Nielsen,[‡] John R. Reynolds,[‡] Klaus Müllen,[†] and Wojciech Pisula*[,†,§]

[†]Max Planck Institute for Polymer Research, Ackermannweg 10, D-55128 Mainz, Germany

[‡]The George and Josephine Butler Polymer Research Laboratory, Center for Macromolecular Science and Engineering, Department of Chemistry, University of Florida, Gainesville, Florida 32611, United States

Supporting Information

ABSTRACT: The organization of a series of phenylene−thienylene-based oligomers solubilized with terminal (ω-hydroxyalkyl) and lateral (alkoxy) side chains was studied. The thermal behavior and self-assembly on the surface during solution and thermal processing are mainly affected by the position and length of the side chains. The molecules organize in different fashions, depending on the substitution pattern, as indicated by fiber X-ray scattering results. The oligomer with only lateral side chains behaves as a typical rigid rod arranged in lamella structures, while those with a homogeneous alkyl mantle around the aromatic system adapt a disklike character and form one-dimensional stacks. Because of the large aromatic rod, the role of the terminal hydroxy groups on the self-assembly can be neglected. The choice of the alkyl density around the aromatic core allows a control over the molecular organization, which is essential for the development of high-performance solution-processable organic semiconductors.

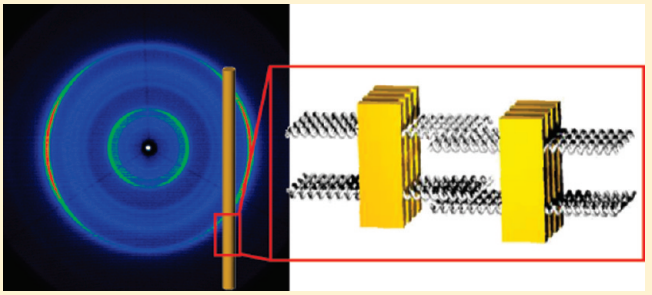

KEYWORDS: phenylene thienylene oligomer, supramolecular organization, wide-angle X-ray scattering, self-assembly

1. INTRODUCTION

Supramolecular assembly of molecular building blocks allows the generation of materials with novel properties. In this approach, small molecules interact noncovalently with each other to form the supramolecular structure. The most frequently applied tools as driving forces for self-assembly are π-stacking interactions through conjugated aromatic units and hydrogen bonds introduced via functional groups.[1] Control over the supramolecular organization can also be established by two additional parameters: local phase separation between molecular fractions of different density and molecular shape of the building blocks.[2] For instance, phase separation occurs for alkyl-substituted conjugated molecules between the soft aliphatic and rigid aromatic parts. For sufficiently long substituents, distinct thermotropic phases can arise.[3] When such alkyl side chains are introduced around a disk-shaped aromatic core, the molecules assemble into columnar stacks, which can serve as one-dimensional charge carrier pathways.[4] Hydrophilic/hydrophobic interactions between these substituents can induce an additional phase separation in the columnar periphery, resulting in more-complex superstructures, including tubular fibers and helical packing.[5] In contrast to a disk shape, rigid rodlike conjugated oligomers with flexible chains typically organize in two-dimensional layered structures, which ensures higher charge carrier mobilities over macroscopic dimensions when compared to columnar stacks.[6] The substitution variety of a rigid rod is larger since the chains can be attached at both lateral and terminal positions of the molecule, which impacts the assembly and thermal properties.[7] Even more diverse organizations, such as columnar, layered, or cubic phases, originate from amphiphilic rodlike segments including t-shaped facial amphiphilic and bolaamphiphilic molecules with terminal hydroxy functionalities capable of forming hydrogen-bonded networks.[8] On the other hand, polycatenar mesogens carrying longer alkyl chains at each end arrange predominantly in columnar assemblies.[9] Recently, it has been shown that the organization of the polycatenar nanostructure is dependent on the number and length of the terminal alkoxy chains, leading to smectic and cubic phases.[10] Time-of-flight charge transport experiments further revealed the largest carrier mobilities for layered organizations, which were attributed to a higher dimensionality of the charge transport, in comparison to a cubic arrangement.

Thiophene- and phenylene−thiophene-based oligomers are well-known organic semiconductors that are potential materials for applications in organic electronics.[11] As a great advantage, these molecules are solution-processed into thin film devices by controlling their solubility, thermal properties, and order by the flexible side chains.[12] As described previously, for some of the cases, such substitution leads to two-dimensional (2D) layered structures and to charge carrier mobilities above 0.1 $cm^2/(V\,s)$ over macroscopic dimensions.[13] The introduction of functional

Received: December 26, 2010
Revised: February 7, 2011
Published: March 01, 2011

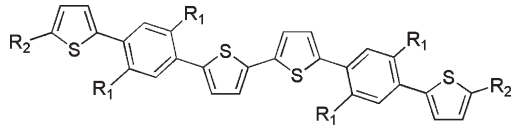

1 $R_1 = OC_7H_{15}$ $R_2 = H$
2 $R_1 = OC_7H_{15}$ $R_2 = (CH_2)_6OH$
3 $R_1 = OC_{12}H_{25}$ $R_2 = (CH_2)_6OH$
4 $R_1 = OC_{16}H_{33}$ $R_2 = (CH_2)_6OH$

Figure 1. Structures of the phenylene−thienylene-based oligomers investigated.

Table 1. Phase-Transition Temperatures from Solid to Isotropic Melt of Oligomers 1−4 (Second Heating by 10 °C/min)

compound	phase transition (°C) [enthalpy (J g^{-1})]
1	97 [30.6]
2	68 [30.6]
3	124 [42.6]
4	123 [46.9]

groups capable of forming hydrogen bonds or cross-links further stabilize the molecular packing in such layers.[14]

Our study focuses on the variation of the supramolecular organization with changing the substitution pattern of 1,4-phenylene-2,5-thienylene (referenced in the text as phenylene−thienylene)-based oligomers (**1**−**4**). The solid-state assembly of these oligomers with attached terminal ω-hydroxyalkyl and lateral alkoxy side chains is compared. Thereby, the terminal substituents carry additional hydroxy groups for hydrogen bonding at the core periphery. Structure analysis based on fiber X-ray scattering indicates a tendency toward a columnar organization when increasing the alkyl mantle density around the rigid aromatic rod. This trend is attributed to a more pronounced local phase separation between the rigid and soft fractions for oligomers with longer side chains. The hydroxy groups do not play a role in the molecular arrangement. Furthermore, the side chains have a strong affect on the morphology formation during deposition from solution and thermal processing.

2. RESULTS AND DISCUSSION

Materials. Four phenylene−thienylene-based oligomers containing laterally and terminally attached side chains of different lengths have been synthesized utilizing a synthetic method similar to that which has been previously described for EDOT-containing analogues (see the Supporting Information for experimental details and full characterization).[15] For this study, the aromatic rod consisting of four 2,5-thienylene units and two 1,4-phenylene units is maintained unchanged, while the substitution pattern is varied. As noted by the structures of the oligomers presented in Figure 1, compound **1** carries alkoxy chains only at the lateral positions of the rigid rod, while compound **2** is substituted additionally by ω-hydroxyalkyls at the termini. Compounds **3** and **4** possess the same terminal ω-hydroxyalkyl substituents, but longer lateral alkoxy chains.

Thermal Properties. In the first step, the influence of the substitution pattern on the thermal behavior of oligomers **1**−**4** was determined by differential scanning calorimetry (DSC) (see Table 1). Except for the cold-crystallization peaks for **1** and **2**, which originate from a too-rapid cooling and a suppressed crystallization during the first cooling, all oligomers reveal only one phase transition during heating, which is related to the isotropization temperature (T_i) (see Figure 2). The incorporation of the terminal side chain containing the hydroxy group reduces the T_i value for **2**, in comparison to **1**. Surprisingly, both **3** and **4** with longer lateral solubilizing groups possess a considerably higher T_i (~124 °C) than **1** and **2**. Typically, an increase of the side chain length decreases the phase temperature.[7] Because of the low T_i value of **2**, in comparison with that of **1**, the effect of hydrogen bonds via the hydroxy functions on the thermal properties of **3** and **4** is minimal. The unusual behavior of **3** and **4** is attributed to their supramolecular organization, which differs from that of **1** and **2** and is discussed in detail in the sections below. Interestingly, **3** and **4** show identical organizations (see the Structural Analysis section below), being in agreement with similar phase transition temperatures and enthalpy values for the two compounds.

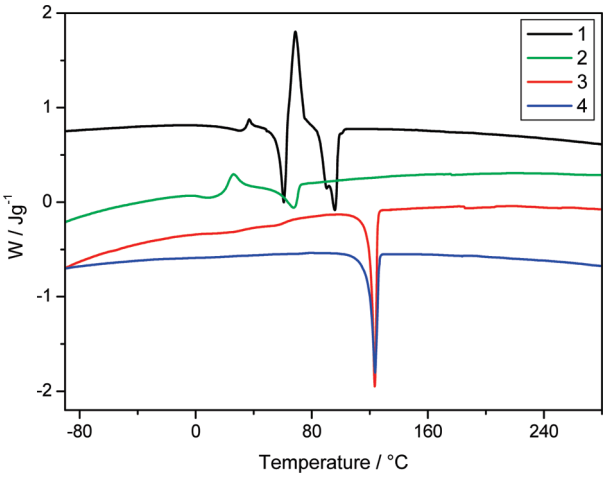

Figure 2. Differential scanning calorimetry (DSC) scans for oligomers **1**−**4** during a second heating at a rate of 10 °C/min.

Morphology from the Isotropic Melt. Based on the above-described thermal data, the morphology after cooling oligomers **1**−**4** from the isotropic melt was studied. The solidification process and morphology formation during cooling provides information about the intermolecular interactions of the building blocks during self-assembly. In this case, the samples were processed as thin films sandwiched between two glass slides, while the morphology was investigated using cross-polarized optical microscopy (POM). All four compounds display highly birefringent optical textures when solidified from the isotropic state at a cooling rate of 1 °C/min, and significant differences in the type of textures between the films are obvious (see Figure 3). Compound **1** shows a poorly defined morphology (see Figure 3a), whereas oligomer **2** with additional terminal side chains shows small, but distinct, spherulitic domains growing under the same processing conditions (see Figure 3b). The incorporation of longer lateral substituents onto the aromatic rod results in even larger domains. Macroscopic spherulites are obvious for **3**, indicating a pronounced self-assembly of the molecules (see Figure 3c). These domains are highly anisotropic and show an extinction along the polarizer directions, as expressed by the Maltese cross. The application of a λ-plate exhibits a distinctive red−blue color distribution in the quarters of the spherulite, which is characteristic for an optically negative material where the refractive index parallel to the radial direction of the

dx.doi.org/10.1021/cm1036716 |Chem. Mater. 2011, 23, 1939–1945

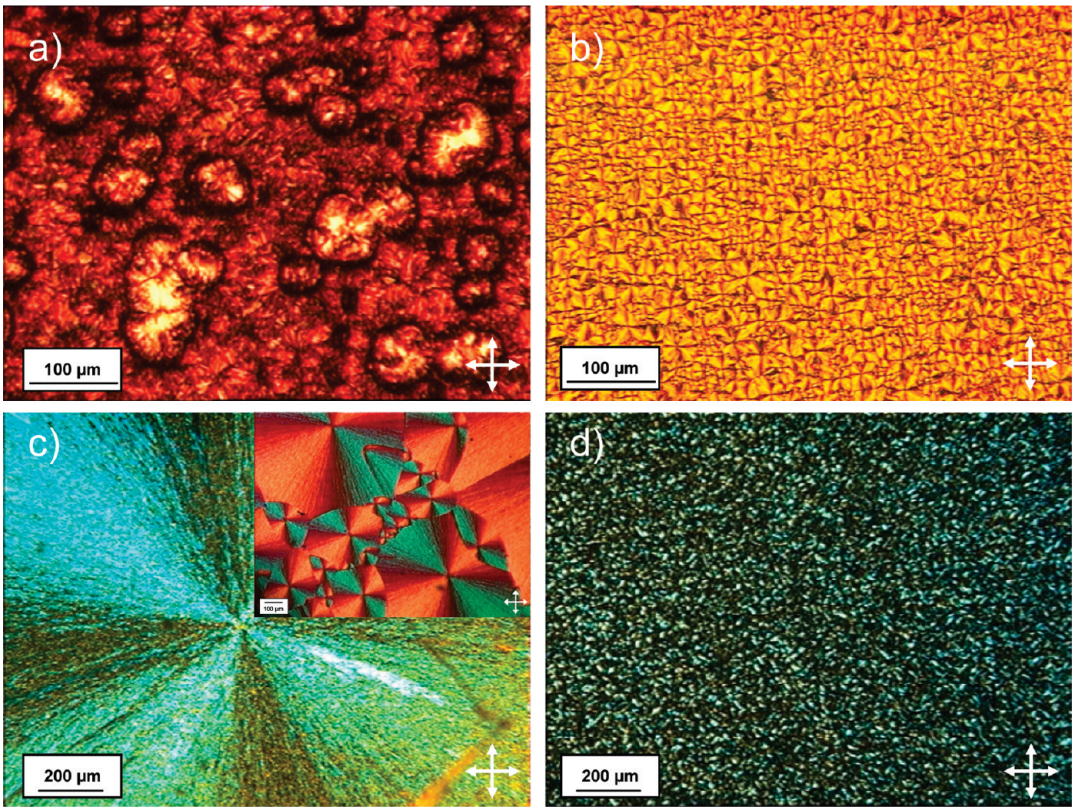

Figure 3. Cross-polarized optical microscopy images of (a) **1**, (b) **2**, (c) **3** (inset with a λ-plate), and (d) **4**. All images were taken at 30 °C after cooling the samples (1 °C/min) from the isotropic melt between two glass slides.

spherulite is smaller than that perpendicular to it. This optical behavior has been reported for columnar discotic molecules, which are long-range-aligned in an edge-on arrangement toward the substrate.[16] In contrast to the trend observed for **1**−**3**, only small crystals arise for **4**, which remain unchanged, even at other cooling rates. The long hexadecyloxy chains of **4** are most likely too sterically demanding and hinder the assembly of the molecules, leading to only small domains.

To conclude this section, the POM study implies a close relationship between domain order and size and the substitution pattern of the molecules. Comparing **1**, **2**, and **3**, a more pronounced long-range organization, and, hence, macroscopically larger domains, are observed as the length of the side chains increases. Most probably, this is a kinetically driven process controlled by the steric hindrance of the side chains as for disklike systems.[17] Longer chains reduce the attractive π-stacking interactions and cause a slower self-assembly of the molecules into the macroscopic textures with extended sizes. However, the very long hexadecyloxy substituents have a negative effect on the morphology formation of compound **4**, which is no longer driven by strong intermolecular $\pi-\pi$ interactions.

Morphology from Solution. Analogous to the processing from the melt, self-assembly on a surface upon solution deposition provides further insight into the molecular interactions and the effect of side-chain length and position.

Thin films were prepared by drop-casting a 0.5 mg/mL toluene solution on a silicon surface, and the topography was inspected by atomic force microscopy (AFM). Usually, longer alkyl chains hinder the molecular interaction, resulting in less-defined structures on the surface. In the case of oligomers **1**−**4**, a more defined morphology appears for the derivatives with longer side chains (Figure 4). For **1**, a relatively rough surface consisting of globular structures is obvious in the AFM image (see Figure 4a), while **2** forms single short fibrous or rodlike structures with lengths between 500 nm and 2 μm (see Figure 4b). These long cylindrical features of uniform height of ca. 200 nm are randomly distributed over the substrate, which might imply their initial assembly in solution. Compounds **3** and **4** reveal a completely different morphology, in comparison to **1** and **2**. Both assemble into a dendritic morphology (see Figures 4c and 4d), but the dendritic domains of **4** (mainly above 1 μm) are significantly larger than those of **3** (mainly below 1 μm). This tendency can be put into correlation with the textures obtained after thermal processing (see the previous section). While **1** precipitates rapidly from the solution, because of strong molecular interactions, compound **2** with additional substitutes at the termini forms anisotropic fibrous micro-objects. Furthermore, oligomers **3** and **4** create larger dendritic structures, because of the larger alkyl mantle, which reduces the kinetics of the assembly process. This hypothesis is in agreement with the structural analysis of the bulk organization in which **3** and **4** with longer side chains showing higher structural order, as indicated by a larger numbers of reflections in the X-ray patterns (see the following section).

Structural Analysis of the Supramolecular Organization. The effect of the alkyl substitution pattern on the packing of the oligomers **1**−**4** was investigated by X-ray scattering, using a 2D detector. The samples were prepared by fiber extrusion, which induces a macroscopic orientation in the specimen. To to ensure reproducibility, the compounds were extruded at different

dx.doi.org/10.1021/cm1036716 |*Chem. Mater.* 2011, 23, 1939–1945

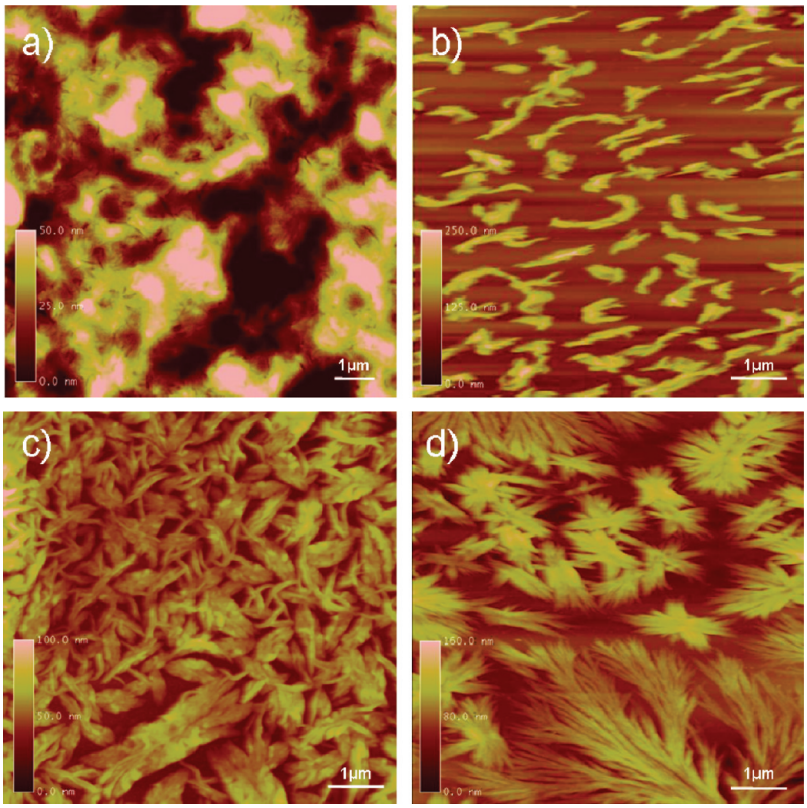

Figure 4. AFM height images of (a) **1**, (b) **2**, (c) **3**, and (d) **4**. All samples were prepared by drop-casting a 0.5 mg/mL toluene solution onto a silicon substrate.

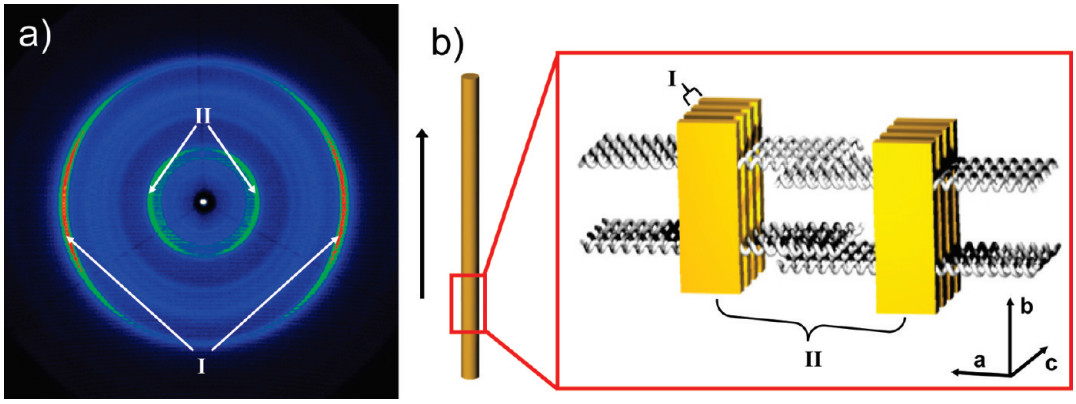

Figure 5. (a) Fiber 2D-WAXS of **1** at 30 °C and (b) schematic illustration of the molecular organization within the extruded fiber. The black arrow indicates the extrusion direction with respect to the 2D pattern and the arranged oligomers.

conditions, changing the draw speed, temperature, and sample thickness. In all cases, the observed organization was insensitive to the processing parameters.

The experiment was carried out with the fiber sample vertical to the 2D detector. This allows for a direct comparison of the molecular alignment toward the orientation, which is coincident with the extrusion direction. Figure 5a shows the 2D wide-angle X-ray scattering (2D-WAXS) pattern for **1** recorded at 30 °C, which did not change within the temperature range of the solid state being in agreement with the investigation of the thermal properties. The pattern can be separated into a meridional and equatorial plane in which the reflections are located. For **1**, only two distinct equatorial reflections, assigned as I and II, are obvious (see Figure 5a). Figure 5b shows the schematic model for the molecular organization of **1** in the extruded fiber. For all samples, the packing parameter *a* is defined along the short oligomer axis and *b* as the long axis, while *c* is related to the π-stacking period. Scattering intensity reflection II, in the midangle range corresponding to a *d*-spacing of 1.0 nm, is attributed to the interlamella distance, taking into account interdigitation of the heptyloxy chains (see Figure 5b). The wide-angle reflection I, correlating to 0.42 nm, is assigned to the intralamella packing period (see Figure 5b). The equatorial position of these two reflections clearly indicates an alignment of the molecules with their long axis along the fiber axis and thus along the extrusion direction. This alignment is

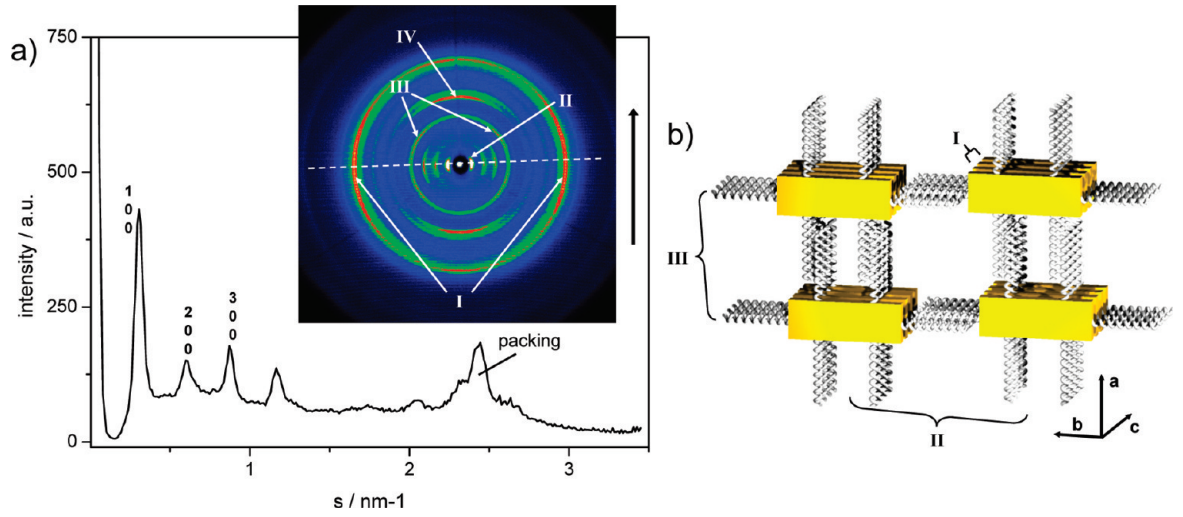

Figure 6. (a) Fiber 2D-WAXS pattern of **2** at 30 °C and the equatorial integration (dashed line), as a function of the scattering vector *s*. Reflections in the plot are indexed by the Miller's indices (*hkl*). (b) Schematic illustration of the organization of **2** in the fiber sample; *d*-spacings are labeled according to the 2D pattern.

characteristic for molecules with a high aspect ratio, such as long rigid rods or conjugated polymers.[18]

When compared to **1**, the 2D pattern of **2** displays a slightly different distribution of the reflections. The main equatorial small-angle reflection, assigned in Figure 6a as II, is attributed to the *d*-spacing of 3.44 nm along the *b*-axis being in good agreement with the calculated molecular length[19] and the terminally attached chains, which increase the distance between molecules. Higher-order 200 and 300 reflections suggest improved order, in comparison to **1**. The wide-angle scattering intensity reflection I in the same plane of the pattern is attributed to the packing period of 0.41 nm of the π-stacked oligomers and is identical to that of compound **1**. The position of both discussed reflections for **2** in the equatorial plane of the pattern implies that the molecules are oriented with their short molecular axis along the fiber axis. This stands in contrast to compound **1**. The distance of 1.24 nm along the short molecular axis coincides with the fiber axis and is represented by the off-meridional reflections (denoted as III). Additional meridional reflections (denoted as IV) are related to a spacing of 0.62 nm and are assigned as high-order 020. From the structural analysis for **2**, a rectangular unit cell has been derived with a = 1.24 nm and b = 3.44 nm. The parameter a is slightly larger than that for **1**, because of the additional lateral side chains and, thus, a denser alkyl mantle around the aromatic core. The organization in the 1D stacks of **2** is schematically illustrated in Figure 6b. Note that the crystal axes a, b, and c are defined in the same way as for **1**. The orientation of **2** with its long axis perpendicular to the fiber direction is correlated to the additional side chains at the terminal position of the rigid rod, in comparison to **1**. Again, this specific molecular alignment is independent of the processing conditions, such as temperature, drawing rate, or fiber diameter, and therefore can be related only to the terminal side chains. These additional substituents change the aspect ratio of the compound and induce a self-assembly into quasi one-dimensional stacks with a rigid core surrounded by flexible chains. To confirm the negligible role of the terminal hydroxy units on the packing, compounds **3** and **4** were investigated in the same way.

Compounds **3** and **4** carry longer lateral dodecyloxy and hexadecyloxy chains, respectively, while the terminal substituents are unchanged. The 2D patterns of both systems show the same reflection distribution, indicating an identical supramolecular arrangement of the molecules (see Figures 7a and 7b). In both cases, the appearance of a large number of higher-order reflections is characteristic for high structural order. The off-meridional (I) and meridional (II) scattering intensities are assigned to a tilting of the molecules, which are packed in one-dimensional (1D) stacks. For **3** and **4**, reflection I corresponds to a stacking distance of 0.40 nm and a molecular tilt angle of ~30° toward the stack axis (see Figure 7c). Meridional reflection II is related to an intrastack period of 0.48 nm of the tilted units (see Figure 7c). Such an intrastack packing of tilted molecules is characteristic for crystalline discotics.[20] The equatorial reflections are due to the arrangement of the stacks, which are aligned along the extruded fiber. For both compounds, the same type of monoclinic unit cell with an angle of γ = 75° between a and b was derived from the positions of the reflections. The parameters are a = 2.26 nm, b = 3.18 nm for **3** and a = 2.72 nm, b = 3.98 nm for **4** (see Figure 7c). The unit-cell size thereby is dependent only on the length of the side chain. The parameter b is in agreement with the long molecular axis, while a, being approximately twice the value found for **1** and **2**, suggests a correlation between every second rigid rod along the a-plane, which originates from a herringbone arrangement, as illustrated in Figure 7c. The increase of the alkyl mantle density results in a gradually larger distance between molecules along the b parameter.

The assembly of **3** and **4** into tilted one-dimensional stacks (which, in contrast to **1** and **2**, are oriented in the extrusion direction of the fiber specimen) is analogous to the behavior of discotics.[4] These stacks are based on the π-interactions between the aromatic cores and the local phase separation between flexible chains and rigid aromatic units. Indeed, the homogeneous decoration of the rigid rod with alkyl substituents induces a disklike character in **3** and **4**. Because of the small aspect ratio of the building block on one hand, and the high aspect ratio of the self-assembled 1D stack on the other, these supramolecular structures align along the orientation (extrusion) direction. This is not the case for **1** and **2**, for which the alkyl mantle around the aromatic core is less dense. Compound **1**, with only lateral side chains and, hence, a much larger molecular aspect ratio,

dx.doi.org/10.1021/cm1036716 |*Chem. Mater.* 2011, 23, 1939–1945

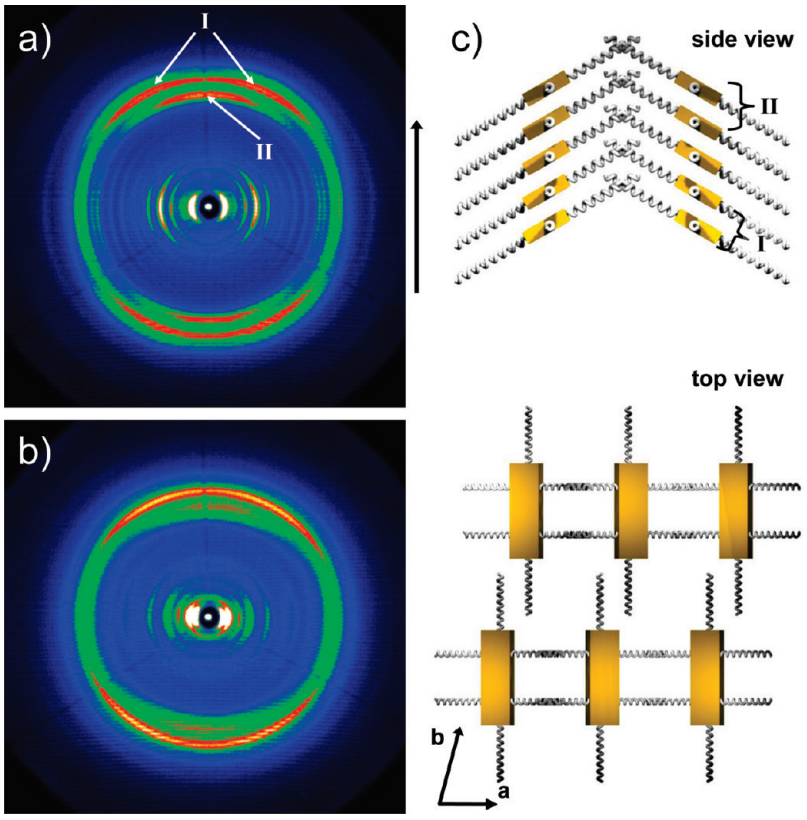

Figure 7. Fiber 2D-WAXS patterns of (a) **3** and (b) **4**, both recorded at 30 °C. (c) Schematic illustration of the organization of **3** and **4**, showing the inside and top view. The reflections are assigned to the corresponding periods in the illustration.

behaves as a typical rigid rod, which arranges in lamella structures oriented along the shearing direction.

■ CONCLUSIONS

For a series of phenylene−thienylene-based oligomers, we have shown that, by controlling the alkyl substitution pattern, we can tune the thermal behavior, solubility, and the solution-processed self-assembly on surfaces. The morphology formation during deposition from solution and thermal processing is a kinetically driven process dominated by the steric hindrance of the side chains. Furthermore, we have shown that side chains change the supramolecular arrangement from lamellar to columnar. The rational choice of the chain length and substitution position at the aromatic rigid rod influences the density of the alkyl mantle and the molecular aspect ratio, changing the molecular character from a typical rigid rod to a disklike building block, as indicated by the structure study on aligned samples. An influence of hydrogen bonds, based on terminal hydroxy functionalities, cannot be detected. This opens a straightforward opportunity to modify and optimize the properties of organic semiconductors based on the same aromatic core simply by adjusting the alkyl mantle.

3. EXPERIMENTAL SECTION

Differential Scanning Calorimetry (DSC). Thermal transition temperatures were determined by differential scanning calorimetry (DSC) (Mettler Toledo, Model DSC822e). Each sample was weighed, using a Mettler M3 microbalance, in standard 40 μL aluminum pans and immediately sealed by a press. The samples underwent a temperature cycle with first heating, first cooling, and second heating at a rate of 10 °C/min (atmosphere, N_2; flow, 35 mL/min) in a wide temperature range (−100 °C to 300 °C). An empty pan was used as a reference. The instrument determined the temperatures of the components and the total heat transferred in any of the observed thermal processes. The enthalpy change associated with each thermal transition was obtained by integrating the area of the relevant DSC peak.

Polarized Optical Microscopy (POM). The optical textures were investigated using a Zeiss West Germany polarizing optical microscopy (POM) device that was equipped with a digital temperature control system (UNKAM TMS 591). Each sample was sandwiched between glass slides to form a thin film and, afterward, was heated above the melting point (see Table 1), using a heating stage. The images were recorded at a temperature of 30 °C between cross-polarizers.

Wide-Angle X-ray Scattering (2DWAXS). The 2D WAXS experiments were performed by means of a rotating anode (Rigaku 18 kW) X-ray beam with pinhole collimation and a 2D Siemens detector. A double graphite monochromator for the Cr Kα radiation (λ = 0.154) was used. The samples were prepared as a thin filament of 0.7 mm in diameter via filament extrusion, using a home-built mini-extruder. The sample was positioned perpendicular to the incident X-ray beam and vertical to the 2D detector, as determined by Bragg's law ($s = (2 \sin \theta)/\lambda$, where the λ is the wavelength of radiation (λ = 0.154 nm) and 2θ the scattering angle).

Atomic Force Microscopy (AFM). The morphology of the compounds was examined using an AFM system (Veeco Digitals Instruments) in the tapping mode at room temperature. The thin films of the samples were prepared by different concentrations of drop-cast or spin-coated films on silicon wafer. The height and phase images were recorded simultaneously while operating the instrument in the tapping mode.

■ ASSOCIATED CONTENT

Supporting Information. Synthetic procedure and all characterizations of **1**−**4**. This material is available free of charge via the Internet at http://pubs.acs.org.

■ AUTHOR INFORMATION

Corresponding Author

*Fax: (+49) 6131-379-100. E-mail: pisula@mpip-mainz.mpg.de.

Present Addresses

§Present address: Evonik Degussa GmbH, Process Technology & Engineering, Process Technology—New Processes, Rodenbacher Chaussee 4, D-63457 Hanau-Wolfgang, Germany.

4. ACKNOWLEDGMENT

The German Science Foundation (Korean-German IR TG), the European Community's Seventh Framework Programme ONE-P (Grant Agreement No. 212311), DFG Priority Program SPP 1355, DFG MU 334/32-1, DFG Priority Program SPP 1459, and ESF Project GOSPEL (Ref. No. 09-EuroGRAPHENE-FP-001). J.R.R. acknowledges funding from the AFOSR (FA9550-09-1-0320).

■ REFERENCES

(1) (a) Brunsveld, L.; Folmer, B. J. B.; Meijer, E. W.; Sijbesma, R. P. *Chem. Rev.* **2001**, *101*, 4071. (b) Hoeben, F. J. M.; Jonkheijm, P.; Meijer, E. W.; Schenning, A. P. H. J. *Chem. Rev.* **2005**, *105*, 1491. (c) Ciferri, A. *Macromol. Rapid Commun.* **2002**, *23*, 511. (d) Pollino, J. M.; Weck, M. *Chem. Soc. Rev.* **2005**, *34*, 193. (e) Gearba, R. I.; Lehmann, M.; Levin, J.; Ivanov, D. A.; Koch, M. H. J.; Barbera, J.; Debije, M. G.; Piris, J.; Geerts, Y. H. *Adv. Mater.* **2003**, *15*, 1614.

(2) (a) Kato, T.; Mizoshita, N.; Kishimoto, K. *Angew. Chem., Int. Ed.* **2006**, *45*, 38. (b) Goodby, J. W.; Saez, I. M.; Cowling, S. J.; Görtz, V.; Draper, M.; Hall, A. W.; Sia, S.; Cosquer, G.; Lee, S.-E.; Raynes, E. P. *Angew. Chem., Int. Ed.* **2008**, *47*, 2754.

(3) (a) *Handbook of Liquid Crystals*; Demus, D., Goodby, J. W., Gray, G.W., Spiess, H.-W., Vill, V., Eds.; Wiley−VCH: Weinheim, Germany, 1998. (b) Pisula, W.; Zorn, M.; Chang, J. Y.; Müllen, K.; Zentel, R. *Macromol. Rapid Commun.* **2009**, *30*, 1179. (c) Yang, S. H.; Hsu, C. S. J. *Polym. Sci., Part A: Polym. Chem.* **2009**, *47*, 2713.

(4) (a) Laschat, S.; Baro, A.; Steinke, N.; Giesselmann, F.; Hägele, C.; Scalia, G.; Judele, R.; Kapatsina, E.; Sauer, S.; Schreivogel, A.; Tosoni, M. *Angew. Chem., Int. Ed.* **2007**, *46*, 4832. (b) Sergeyev, S.; Pisula, W.; Geerts, Y. H. *Chem. Soc. Rev.* **2007**, 1902. (c) Kumar, S. *Chem. Soc. Rev.* **2006**, *35*, 83.

(5) (a) Sakurai, T.; Shi, K.; Sato, H.; Tashiro, K.; Osuka, A.; Saeki, A.; Seki, S.; Tagawa, S.; Sasaki, S.; Masunaga, H.; Osaka, K.; Takata, M.; Aida, T. *J. Am. Chem. Soc.* **2008**, *130*, 13812. (b) Yamamoto, Y.; Fukushima, T.; N.; Saeki, A.; Seki, S.; Tagawa, S.; Ishii, N.; Aida, T. *J. Am. Chem. Soc.* **2007**, *129*, 9276. (c) Yamamoto, Y.; Fukushima, T.; Suna, Y.; Ishii, N.; Saeki, A.; Seki, S.; Tagawa, S.; Taniguchi, M.; Kawai, T.; Aida, T. *Science* **2006**, *314*, 1761. (d) Feng, X.; Pisula, W.; Kudernac, T.; Wu, D.; Zhi, L.; De Feyter, S.; Müllen, K. *J. Am. Chem. Soc.* **2009**, *131*, 4439. (e) Feng, X.; Marcon, V.; Pisula, W.; Hansen, M. R.; Kirkpatrick, J.; Grozema, F.; Andrienko, D.; Kremer, K.; Müllen, K. *Nat. Mater.* **2009**, *8*, 421.

(6) (a) Murphy, A. R.; Fréchet, J. M. J. *Chem. Rev.* **2007**, *107*, 1066. (b) Yazaki, S.; Funahashi, M.; Kato, T. *J. Am. Chem. Soc.* **2008**, *130*, 13206. (c) Funahashi, M.; Zhang, F.; Tamaoki, N. *Adv. Mater.* **2007**, *19*, 353. (d) van Breemen, A. J. J. M.; Herwig, P. T.; Chlon, C. H. T.; Sweelssen, J.; Schoo, H. F.M.; Setayesh, S.; Hardeman, W. M.; Martin, C. A.; de Leeuw, D. M.; Valeton, J. J. P.; Bastiaansen, C. W. M.; Broer, D. J.; Popa-Merticaru, A. R.; Meskers, S. C. J. *J. Am. Chem. Soc.* **2006**, *128*, 2336. (e) Luo, J.; Qu, H.; Yin, J.; Zhang, X.; Huang, K.-W.; Chi, C. *J. Mater. Chem.* **2009**, *19*, 8202.

(7) Yatabe, T.; Suzuki, Y.; Kawanishi, Y. *J. Mater. Chem.* **2008**, *18*, 4468.

(8) (a) Prehm, M.; Götz, G.; Bäuerle, P.; Liu, F.; Zeng, X.; Ungar, G.; Tschierske, C. *Angew. Chem., Int. Ed.* **2007**, *46*, 7856. (b) Tschierske, C. *Chem. Soc. Rev.* **2007**, *36*, 1930. (c) Chen, B.; Zeng, X. B.; Baumeister, U.; Diele, S.; Ungar, G.; Tschierske, C. *Angew. Chem., Int. Ed.* **2004**, *43*, 4621. (d) Prehm, M.; Liu, F.; Zeng, X.; Ungar, G.; Tschierske, C. *J. Am. Chem. Soc.* **2008**, *130*, 14922. (e) Cheng, X.; Prehm, M.; Das, M. K.; Kain, J.; Baumeister, U.; Diele, S.; Leine, D.; Blume, A.; Tschierske, C. *J. Am. Chem. Soc.* **2003**, *125*, 10977.

(9) (a) Hoag, B. P.; Douglas, L. G. *Adv. Mater.* **1998**, *10*, 1546. (b) Yasuda, T.; Kishimoto, K.; Kato, T. *Chem. Commun.* **2006**, 3399.

(10) Yasuda, T.; Ooi, H.; Morita, J.; Akama, Y.; Minoura, K.; Funahashi, M.; Shimomura, T.; Kato, T. *Adv. Funct. Mater.* **2009**, *19*, 411.

(11) (a) Mishra, A.; Ma, C.-Q.; Bäuerle, P. *Chem. Rev.* **2009**, *109*, 1141. (b) Hajlaoui, R.; Fichou, D.; Horowitz, G.; Nessakh, B.; Constant, M.; Garnier, F. *Adv. Mater.* **1997**, *9*, 557. (c) Fichou, D. *J. Mater. Chem.* **2000**, *10*, 571. (d) Garnier, F.; Hajlaoui, R.; El Kassmi, A.; Horowitz, G.; Laigre, L.; Porzio, W.; Armanini, M.; Provasoli, F. *Chem. Mater.* **1998**, *10*, 3334. (d) Vaidyanathan, V.; Doetz, F.; Katz, H. E.; Lawrentz, R.; Granstrom, J.; Reichmanis, E. *Chem. Mater.* **2007**, *19*, 4676.

(12) (a) Ellinger, S.; Kreyes, A.; Ziener, U.; Hoffmann-Richter, C.; Landfester, K.; Möller, M. *Eur. J. Org. Chem.* **2007**, 5686. (b) Ellinger, S.; Ziener, U.; Thewalt, U.; Landfester, K.; Möller, M. *Chem. Mater.* **2007**, *19*, 1070. (c) Ponomarenko, S. A.; Kirchmeyer, S.; Elschner, A.; Alpatova, N. M.; Halik, M.; Klauk, H.; Zschieschang, U.; Schmid, G. *Chem. Mater.* **2006**, *18*, 579. (d) Katz, H. E.; Laquindanum, J. G.; Lovinger, A. J. *Chem. Mater.* **1998**, *10*, 633. (e) Mushrush, M.; Facchetti, A.; Lefenfeld, M.; Katz, H. E.; Marks, T. J. *J. Am. Chem. Soc.* **2003**, *125*, 9414. (f) Zhang, S.; Guo, Y.; Wang, L.; Li, Q.; Zheng, K.; Zhan, X.; Liu, Y.; Liu, R.; Wan, L.i-J. *J. Phys. Chem. C* **2009**, *113*, 16232.

(13) (a) Halik, M.; Klauk, H.; Zschieschang, U.; Schmid, G.; Ponomarenko, S.; Kirchmeyer, S.; Weber, W. *Adv. Mater.* **2003**, *15*, 917. (b) Funahashi, M.; Zhang, F.; Tamaoki, N. *Adv. Mater.* **2007**, *19*, 353.

(14) (a) McCulloch, I.; Coelle, M.; Genevicius, K.; Hamilton, R.; Heckmeier, M.; Heeney, M.; Kreouzis, T.; Shkunov, M.; Zhang, W. *Jpn. J. Appl. Phys.* **2008**, *47*, 488. (b) Kreouzis, T.; Baldwin, R. J.; Shkunov, M.; McCulloch, I.; Heeney, M.; Zhang, W. *Appl. Phys. Lett.* **2005**, *87*, 172110.

(15) Nielsen, C. B.; Angerhofer, A.; Abboud, K. A.; Reynolds, J. R. *J. Am. Chem. Soc.* **2008**, *130*, 9734.

(16) Shen, H.; Jeong, K.-U.; Graham, M. J.; Leng, S.; Huang, H.; Lotz, B.; Hou, H.; Harris, F. W.; Cheng, S. Z. D. *J. Macromol. Sci., Part B: Phys.* **2006**, *45*, 215. (b) Pisula, W.; Kastler, M.; Wasserfallen, D.; Pakula, T.; Müllen, K. *J. Am. Chem. Soc.* **2004**, *126*, 8074.

(17) (a) Pisula, W.; Dierschke, F.; Müllen, K. *J. Mater. Chem.* **2006**, *16*, 4058. (b) Kastler, M.; Pisula, W.; Laquai, F.; Kumar, A.; Davis, R.; Wasserfallen, D.; Garcia Gutiérrez, M. C.; Butt, H.-J.; Riekel, C.; Wegner, G.; Müllen, K. *Adv. Mater.* **2006**, *18*, 2255.

(18) (a) Beaujuge, P. M.; Pisula, W.; Tsao, H. N.; Ellinger, S.; Müllen, K.; Reynolds, J. R. *J. Am. Chem. Soc.* **2009**, *131*, 7514. (b) Wang, Y.; Watson, M. D. *Macromolecules* **2008**, *41*, 8643.

(19) A length of ca. 2.3 nm was determined for the aromatic core based upon theoretical calculations (AM1), using SPARTAN PRO.

(20) Pisula, W.; Kastler, M.; Wasserfallen, D.; Mondeshki, M.; Piris, J.; Schnell, I.; Müllen, K. *Chem. Mater.* **2006**, *18*, 3634.